

Convective Instability Driven by Diffusiophoresis of Colloids in Binary Liquid Mixtures

Carmine Anzivino, Klejdis Xhani, Marina Carpineti, Stefano Verrastro, Alessio
Zaccone,* and Alberto Vailati*

*Department of Physics “A. Pontremoli”, University of Milan, via Celoria 16, 20133 Milan,
Italy*

E-mail: alessio.zaccone@unimi.it; alberto.vailati@unimi.it

Abstract

ABSTRACT: In a binary fluid mixture, the concentration gradient of a heavier molecular solute leads to a diffusive flux of solvent and solute to achieve thermodynamic equilibrium. If the solute concentration decreases with height, the system is always in a condition of stable mechanical equilibrium against gravity. We show experimentally that this mechanical equilibrium becomes unstable in case colloidal particles are dispersed uniformly within the mixture, and that the resulting colloidal suspension undergoes a transient convective instability with the onset of convection patterns. By means of a numerical analysis, we clarify the microscopic mechanism from which the observed destabilisation process originates. The solute concentration gradient drives an upward diffusiophoretic migration of colloids, in turn causing the development of a mechanically unstable layer within the sample, where the density of the suspension increases with height. Convective motions arise to minimize this localized rise in gravitational potential energy.

A spontaneous drift motion of colloidal particles in a binary fluid mixture can be caused by the concentration gradient of a molecular solute¹⁻⁴. This process, commonly named

diffusiophoresis, has found many applications in the last years, which include the microfluidic separation of colloids^{5,6}, the colloidal self-assembly⁷ and the motion of self-propelled nanoparticles⁸⁻¹⁰. Within this context, an increasing number of studies have investigated how to exploit diffusiophoresis for controlling the motion of dispersed particles in porous media and dead-end channels¹¹⁻¹⁴, with particular emphasis to the quest of novel strategies for improving current particle manipulation capability^{15,16}. Very little attention has been paid, instead, to the implications of diffusiophoretic migration on the gravitational stability of colloidal suspensions. Yet this phenomenon appears to be crucial for particle manipulation in conditions where gravitational effects cannot be neglected, and to elucidate on outstanding problems such as the origin of the chaotic motion of catalytic particles¹⁷ and of pattern formation in biological systems^{18,19}.

In this Letter, we experimentally address the question of whether diffusiophoresis can lead a colloidal suspension towards a convective instability. We consider the case of silica nanospheres (LUDOX TMA, 22 nm diameter) uniformly dispersed in a fluid binary mixture in which a transient concentration gradient of molecular solute is produced by interdiffusion²⁰. More specifically, a layer of colloids in water is brought in contact from above with a layer of colloids dispersed at the same volume fraction in a water-glycerol mixture, and glycerol and water molecules are allowed to diffuse into each other to achieve thermodynamic equilibrium (Fig. 1(a)). In the absence of dispersed colloids, the arranged system is always in a condition of stable mechanical equilibrium attained by layering the glycerol so that the overall density of the mixture decreases with height²¹. In this configuration, a small parcel of fluid displaced upwards by a perturbation becomes surrounded by fluid of smaller density, and this determines a restoring downward buoyancy force able to inhibit the onset of convective motions^{22,23}. When colloidal particles are distributed uniformly within the mixture, instead, we find that a convective instability arises in the system under generic conditions. This finding is intriguing because the onset of a convective instability requires the accumulation and minimization of gravitational potential energy, as occurs in the unsta-

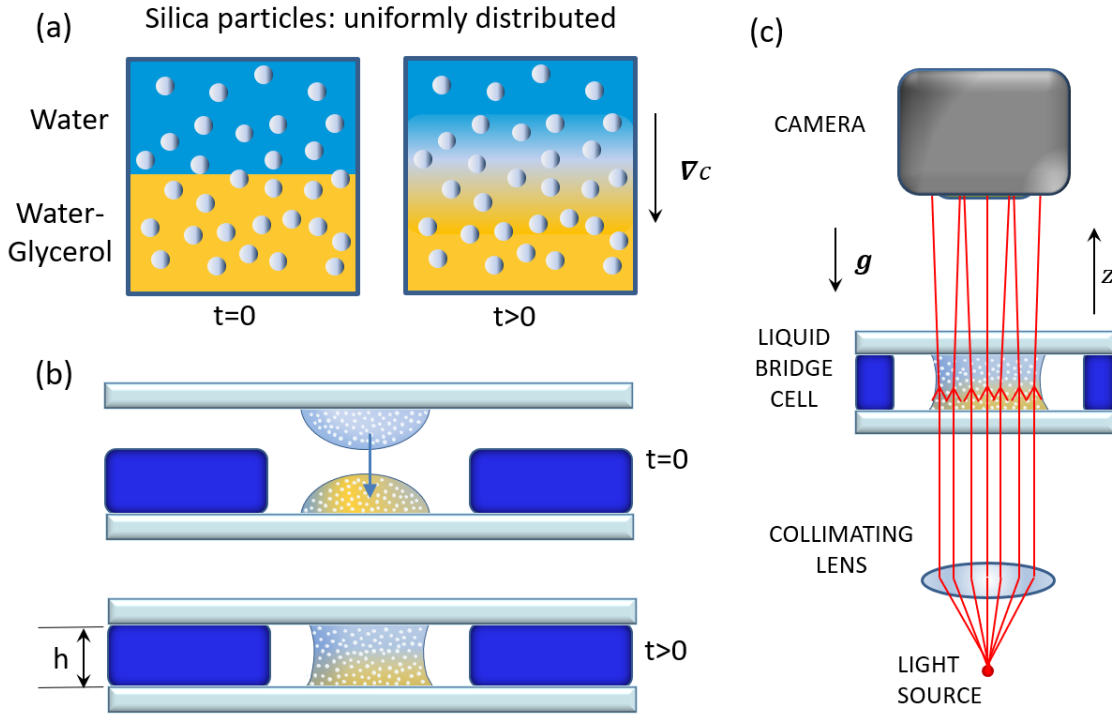


Figure 1: (a) Conceptual scheme of the experiment: at time $t=0$ (left panel) a layer of water is brought into contact with a layer of a water-glycerol mixture. The two liquid phases contain silica particles with uniform volume fraction. As time goes by, the two liquid phases diffuse one into each other. (b) Liquid bridge experimental cell: at $t=0$ one drop of water and one of the water-glycerol mixture are deposited on two microscope glass slides and brought close to each other (top panel). The two droplets coalesce and form a liquid bridge (bottom panel); (c) conceptual scheme of the shadowgraph optical setup: the light emitted by a LED is collimated by an achromatic doublet, crosses the liquid bridge cell in the vertical direction, and is eventually collected by a CMOS camera.

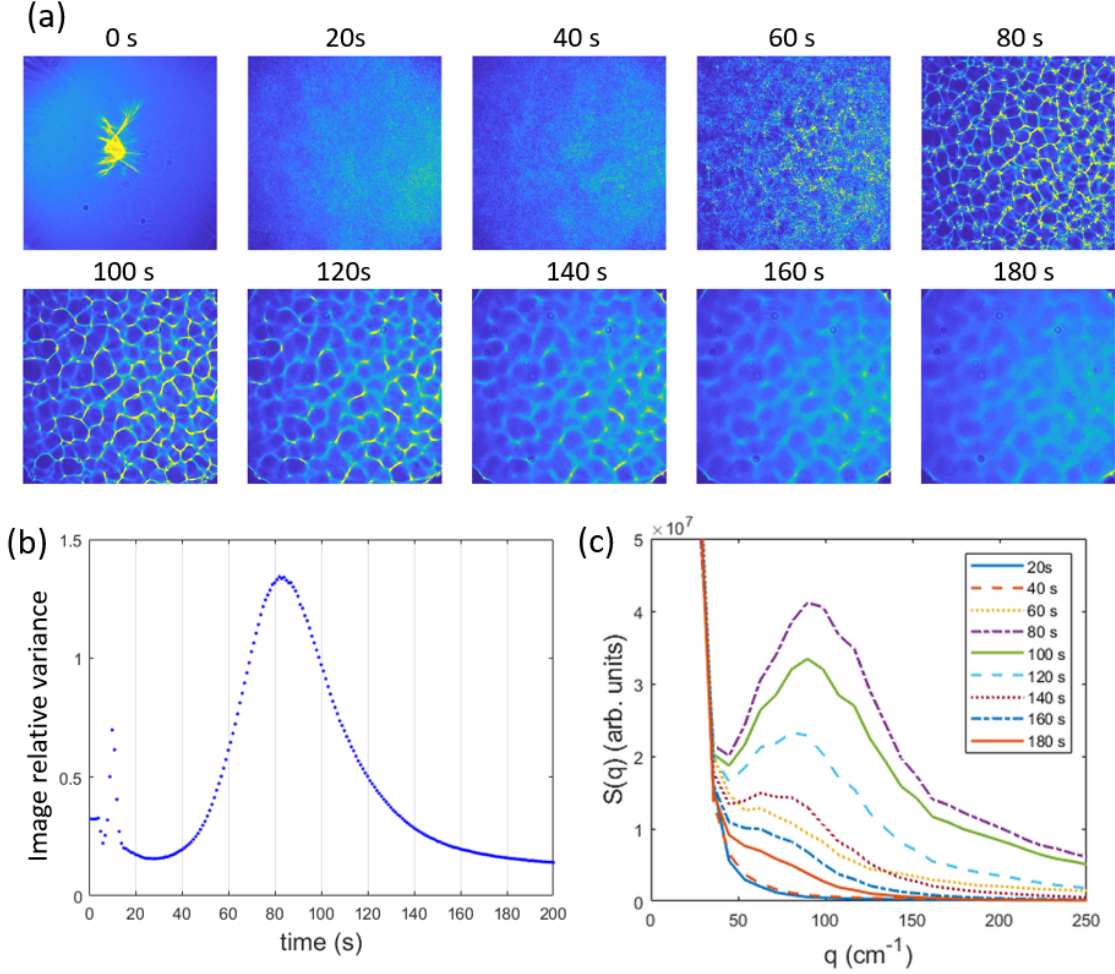


Figure 2: (a - b) Transient convective instability arising in a suspension of 22 nm diameter silica spheres uniformly dispersed (with colloid packing fraction $\phi_0 = 8\%$) within a stratified water-glycerol mixture. The glycerol displays a time-dependent, vertically decreasing, concentration profile (Fig. 1) and its mass fraction present on the bottom of the sample at $t = 0$ is $c_0 = 56\%$. (a) A sequence of shadowgraph images (side of each panel is 7.0 mm in real space) acquired in the interval of time $0 \text{ s} \leq t \leq 180 \text{ s}$ shows the instability planform to consist of disordered cellular patterns which develop at $t_s \approx 60 \text{ s}$, reach a maximum of contrast at $t_{\text{max}} \approx 80 \text{ s}$, and gradually fade away after 100 s. The relative variance σ^2 , (b), and the power spectrum, (c), rapidly increase as a function of time until they are maximised at $t_{\text{max}} \approx 80 \text{ s}$, and decrease continuously for $t > t_{\text{max}}$.

ble configuration where the density of the fluid increases with height²⁴. In the suspension investigated here, instead, the potential energy is minimized due to the mechanically stable stratification of density determined by the glycerol, and no convection is expected to occur^{22,25}. Since the concentration of the colloid is uniform, also the onset of double diffusion convection²⁶ can be safely ruled out.

To address this surprising observation, we numerically investigate the evolution of the base state of the system towards the instability and prove that a key role in the observed destabilisation process is played by the diffusiophoretic migration of colloids induced by the glycerol concentration gradient. We discuss the subtle mechanism through which diffusiophoresis is able to overturn the condition of stable mechanical equilibrium initially determined in the suspension by layering a heavier solute (glycerol) lying below a lighter solvent (water). To perform experiments, we employed a custom cell recently developed by our group²⁷, which is based on the concept of a liquid bridge²⁸, and allows one to bring two miscible liquid phases into contact to start a diffusive process while simultaneously avoiding the formation of spurious perturbations at the liquid-liquid interface. The cell is composed by two standard microscope glass slides placed one on top of the other (Fig. 1(b)). One of them is positioned horizontally on a stage anchored to an optical bench. A rubber spacer (Witte Blaue Matte) of thickness $h = 0.95$ mm is placed on top of this slide to minimize sample evaporation during the experiments. The second slide is placed above the first one, at a distance larger than h . A $37 \mu\text{l}$ droplet of water-Ludox suspension (colloid volume fraction ϕ_0) is anchored to the bottom of the upper slide, while another droplet of water-glycerol-Ludox mixture (colloid volume fraction ϕ_0 and glycerol mass fraction c_0) is deposited on the top of the lower slide. The upper slide is then shifted vertically by using a carriage so that the two drops are brought in contact and a liquid bridge forms between them. Patterns forming inside the sample are visualized using a shadowgraphy setup²⁹ (Fig. 1(c)). A superluminescent diode (SLD) of wavelength 675 ± 13 nm coupled to an optical fiber generates a diverging beam which is collimated on the sample by an achromatic doublet with focal length 10 cm.

After crossing the cell, at a distance of 40 mm from it, the beam impinges on the sensor of a CMOS NX-S4 camera (IDT Vision) with a resolution of 1024x1024 pixel and a 10-bit depth.

A diffusive process starts as soon as the droplets come into contact. This instant represents the starting configuration of each measurement. Experiments are performed at room temperature under isothermal conditions, at fixed combinations (ϕ_0, c_0) , where ϕ_0 is varied in the range $\{1\% - 8\%\}$ and c_0 in the range $\{7\% - 56\%\}$. For each measurement, a liquid bridge cell of the kind described above was prepared. Tests performed with tracer particles excluded the presence of Marangoni flow induced by the concentration gradient of the molecular solute at the free surface of the liquid bridge. For each fixed concentration (ϕ_0, c_0) , starting from $t = 0$, a sequence of 2000 images was acquired at a frequency of 1 Hz. A typical sequence of images, collected at $\phi_0 = 8\%$ and $c_0 = 56\%$, shows the development of an instability after a latency time of about $t_s \approx 60$ s (Fig. 2a)). The planform of the instability features a disordered cellular pattern, which reaches maximum contrast shortly after the onset at a time $t_{\max} \approx 80$ s and gradually fades away in a time of the order of 100 s. A similar scenario is observed for all the other combinations of ϕ_0 and c_0 (see Fig. S1 of the Supporting Information (SI)³⁰). In shadowgraph images, bright features are associated with regions where colloid concentration is higher (colloid rich regions act as positive focal length lenses) while dark features map colloid poor regions³¹. Hence, the strength of the convective patterns can be quantified through the relative variance of an image defined as $\sigma^2(t) \equiv \langle (I(\mathbf{x}, t) - \langle I(\mathbf{x}, t) \rangle)^2 \rangle / \langle I(\mathbf{x}, t) \rangle^2$, where $I(\mathbf{x}, t)$ is the intensity of light acquired by the pixel set at position $\mathbf{x} = (x, y)$ and the average $\langle \dots \rangle$ is performed over all the pixels of the image. For each concentration (ϕ_0, c_0) , the relative variance of the acquired sequence of shadowgraph images can be observed to rapidly increase as a function of time until a maximum $\sigma^2(t_{\max})$ is reached at t_{\max} , and then to decrease for $t > t_{\max}$ (Fig. 2(b)) and Fig. S2 of the SI³⁰). An analogous behaviour as a function of time is shown, in correspondence to an unstable mode q_{peak} , by the azimuthally averaged structure factor $S(q, t)$ associated to the acquired shadowgraph images (Fig. 2(c)) .

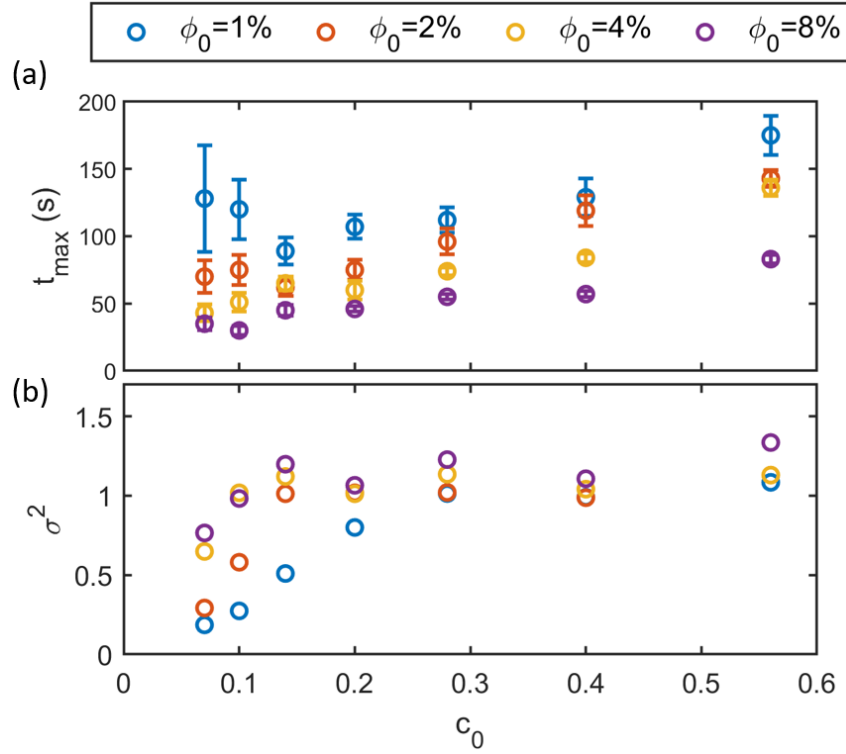


Figure 3: (a) experimentally measured time needed to reach peak variance t_{\max} and (b) relative variance $\sigma^2(t_{\max})$ of shadowgraph images, plotted as a function of ϕ_0 and c_0 . When increasing ϕ_0 at fixed values of c_0 , t_{\max} decreases while $\sigma^2(t_{\max})$ increases. By contrast, at fixed values of ϕ_0 , both t_{\max} and $\sigma^2(t_{\max})$ increase as a function of c_0 .

In order for the observed instability to arise, the system must be driven to a condition where, at least locally, its density increases with height. As temperature is kept constant in our experiments, the driving mechanism cannot be the fluid thermal expansion (such as in the Rayleigh-Bénard convection²⁴) but rather an internal motion of colloids which, however, cannot be the free diffusion as at the beginning of each experiment the colloid concentration in our sample is uniform. Since an upward accumulation of colloidal particles in our system is only originated by the glycerol concentration gradient via diffusiophoresis, the latter must be the main responsible for the destabilization process. In particular the proportionality, expected in nonelectrolyte systems^{32,33}, of the upward diffusiophoretic flux of colloids to both the colloid volume fraction and the strength of glycerol concentration gradient offers a simple explanation for the experimentally observed behaviour of t_{\max} and $\sigma^2(t_{\max})$ as a function of ϕ_0 and c_0 (Fig. 3). t_{\max} decreases when increasing ϕ_0 at fixed values of c_0 because a larger amount of nanoparticles accumulating towards the top of the sample results in the reduction of the time required for the appearance of a vertically increasing density profile in the suspension and, consequently, for the onset and the full development of the convection. To understand the increase of t_{\max} as a function of c_0 at fixed values of ϕ_0 , instead, it must be considered that the increase of c_0 not only enhances the amount of migrating colloids due to diffusiophoresis, but also the density of the glycerol present on the bottom of the sample. A larger number of colloidal particles has to be transferred upwards to destabilize the system in this case, and the time required for the onset and the full development of the instability increases accordingly. The strength of the convective patterns, quantified by $\sigma^2(t_{\max})$, increases as a function of both ϕ_0 and c_0 , as in both cases the patterns involve the motion of a larger number of nanoparticles.

To support the hypothesis above, we performed a theoretical analysis of the evolution of the base state towards the instability. Since the geometry of the experimental sample can be approximated with a cylinder of height $h = 0.95$ mm and diameter $d \gg h$, we introduce a 1D reference system with the $\hat{\mathbf{z}}$ -axis pointing upward. We write the equation for the evolution

of the base state as

$$\begin{aligned}\partial c(z, \tau)/\partial \tau &= (D_1/D_2)h^2 \nabla^2 c(z, \tau), \\ \partial \phi(z, \tau)/\partial \tau &= h^2 \nabla \cdot (\nabla \phi(z, \tau) + \alpha \phi(z, \tau) \nabla c(z, \tau)),\end{aligned}\tag{1}$$

where $\nabla \equiv \partial/\partial z$, while $c(z, \tau)$ and $\phi(z, \tau)$ indicate the spatial profiles of the glycerol mass fraction and of the colloid volume fraction, respectively, at dimensionless times $\tau \equiv D_2 t/h^2$. D_1 and D_2 are the diffusion coefficients of glycerol in water and of colloidal spheres in a water-glycerol mixture, respectively. We treat the diffusiophoretic coefficient α as a “free” parameter quantifying the strength of the diffusiophoretic coupling $\phi \nabla c$. A meaningful value to α can be attributed by comparing theoretical and experimental results.

We apply the Neumann (zero-flux) boundary conditions $(\partial c/\partial z)_{z=0} = (\partial c/\partial z)_{z=h} = 0$ and $(\partial \phi/\partial z)_{z=0} = (\partial \phi/\partial z)_{z=h} = 0$. As initial conditions, we assume $c(z, \tau = 0) = c_0$ for $0 \leq z/h \leq 0.5$ and $c(z, \tau = 0) = 0$ for $0.5 < z/h \leq 1$, while we consider $\phi(z, \tau = 0) = \phi_0$ for $0 \leq z/h \leq 1$. We hence solve the system (1) for many combinations of α , c_0 and ϕ_0 .³⁴ We use data from Ref.³⁵ to fix D_1 and the Stokes-Einstein formula to compute D_2 .³⁶ The same values considered in experiments are chosen for c_0 and ϕ_0 . The main goal of our theoretical analysis is to understand whether the diffusiophoretic term $\alpha \phi \nabla c$ in Eqs. (1) is able to drive the base state towards a mechanically unstable configuration, a task which requires having access to the time evolution of the density profile of the suspension. The latter, for any solution $c(z, \tau)$ and $\phi(z, \tau)$ of system (1), is given by (see SI³⁰) $\rho(c, \phi) = \rho_0 + (\rho_L - \rho_0)\phi + \beta(1 - \phi)c$, where ρ_0 is the density of the solvent in the absence of glycerol molecules, $\rho_L = 2.2 \text{ g/cm}^3$ is the density of a single colloidal particle, and $\beta \equiv d\rho_B/dc$ is the solutal expansion coefficient of a water-glycerol mixture of density ρ_B . For a combination (ϕ_0, c_0) at fixed $\alpha \neq 0$, glycerol starts diffusing upwards when $\tau > 0$ (Fig. 4a)). Simultaneously, colloids gradually deplete from the bottom half of the cell and accumulate towards the top half (Fig. 4(b)). This colloid migration, initially located in the central region of the sample where the concentration gradient of the glycerol is the largest, has relevant repercussions on the overall density

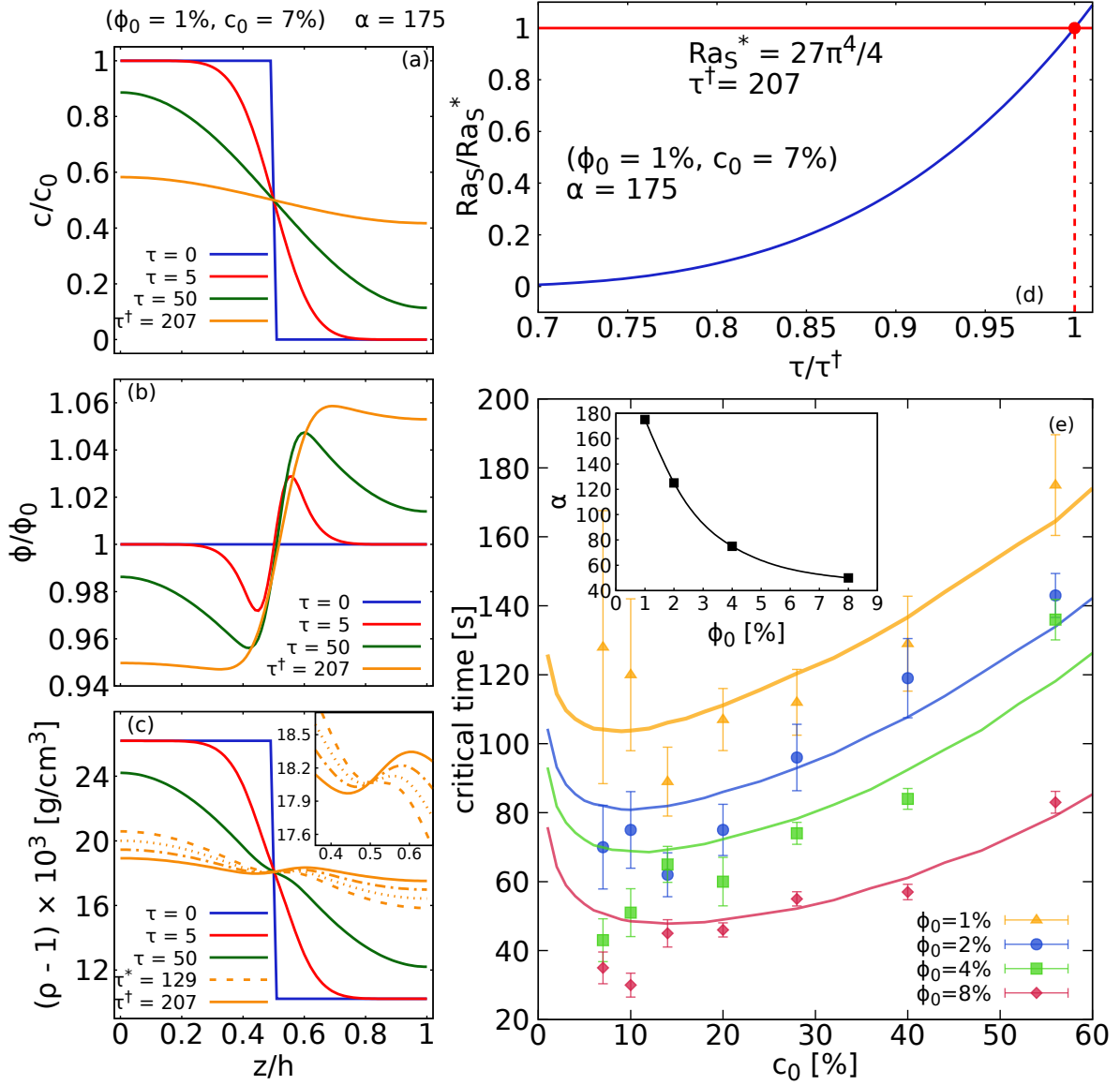


Figure 4: Glycerol mass fraction c (a), colloid volume fraction ϕ (b) and total density of the suspension ρ (c) as a function of the z coordinate of the sample in Fig. 1, for several dimensionless times $\tau \equiv D_2 t/h^2 \geq 0$. Profiles are computed numerically at fixed ($\phi_0 = 1\%$, $c_0 = 7\%$) and $\alpha = 175$. The height of the sample is $h = 0.95$ mm and the value $D_2 = 1.794 \times 10^{-7}$ cm²·s⁻¹ is assumed for the diffusion coefficient of colloids in the water-glycerol mixture. The upward accumulation of colloids, driven by the concentration gradient of glycerol via diffusiophoresis, causes the slope of ρ to display a local inversion after a time $\tau^* = 129$ (inset of (c)). (d) By associating a solutal Rayleigh number (Ra_s) to the density profiles at $\tau \geq \tau^*$, an instability is detected at $\tau^\dagger = 207$, when Ra_s reaches the critical value $Ra_s^* = 27\pi^4/4$. (e) For several combinations of ϕ_0 and c_0 , after properly choosing α , this strategy leads to values of τ^\dagger (lines) in very good agreement with the experimental data of t_{\max} from Fig. 3(a) (points).

profile of the suspension. After a time τ^* , indeed, ρ develops a local minimum ρ_{\min} at a height z_{\min} , followed by a local maximum ρ_{\max} at a height $z_{\max} > z_{\min}$ (Fig. 4(c)). At any $\tau \geq \tau^*$, gravity acts as to pull denser fluid parcels between z_{\min} and z_{\max} from the top to the bottom, and is opposed by the viscous damping force of the fluid. Following Ref.³⁷, we quantify the competition between these two opposite effects by means of a *solutal* Rayleigh number $\text{Ra}_s \equiv g(\Delta z)^3 \Delta \rho / (\eta D_2)$, where $\Delta z \equiv z_{\max} - z_{\min}$, $\Delta \rho \equiv \rho_{\max} - \rho_{\min}$, g is the gravity acceleration, η is the viscosity of the water-glycerol mixture and (again) we compute D_2 via the Stokes-Einstein formula. The increase of Ra_s with time (Fig. 4(d)), which follows from that of Δz and $\Delta \rho$, signals the growing importance of the destabilizing effect of gravity in our system. The latter is hence driven towards a convective instability. For several combinations of ϕ_0 and c_0 , we can obtain an estimate of the “critical” time τ^\dagger at which the instability sets in by using the threshold value $\text{Ra}_s^* = 27\pi^4/4$ associated to isothermal and free boundary conditions³⁸. When α is properly chosen, a good agreement between theoretical curves for $\tau^\dagger(c_0)h^2/D_2$ and experimental data for $t_{\max}(c_0)$ is found for each ϕ_0 (Fig. 4(e)). For comparison we rely on t_{\max} rather than on the time t_s at which patterns start forming, since the former instant is typically more clearly identifiable in a plot of the time evolution of the relative variance (Fig. 2(b)). A general feature of τ^\dagger when plotted as a function of c_0 at fixed values of ϕ_0 and α , is that it exhibits a minimum at $c_0 \approx 7\%$ (Fig. 4(e)), which thus represents the characteristic glycerol concentration that maximizes the efficiency of the diffusiophoretic process in competition to the stabilizing solvent profile and leads to a minimization of the time needed for the onset of the instability.

Overall, fulfillment of the condition $\tau^\dagger h^2/D_2 \approx t_{\max}$ at fixed concentrations (ϕ_0, c_0) can be regarded as a procedure to attribute a meaningful value to the diffusiophoretic mobility coefficient α . In other words, for a given curve $\tau^\dagger(c_0)$ at a fixed ϕ_0 , the value of α can be extracted by requiring that τ^\dagger (expressed in proper units) is compatible with the time t_{\max} experimentally measured for that combination. Since inter-colloids interaction are not taken into account in Eqs. (1), this procedure is only strictly rigorous in the limit $\phi \rightarrow 0$

where a “bare” value α_b is obtained. In the most diluted among the experimentally studied cases, $\phi_0 = 1\%$, we find $\alpha_b \approx 175$, a best-fitting value on the same order of magnitude of $D_1/D_2 \approx 100$. Remarkly, this finding is compatible with recent observations reported within the context of colloid diffusiophoresis driven by the concentration gradient of an electrolyte³⁹, where theoretical modelling and microfluidics experiments have shown the ambipolar diffusivity of the solvent to represent an upper bound for the diffusiophoretic mobility. Our results suggest that a similar relation could apply also to diffusiophoresis in nonelectrolytic systems, without any signature of the super-diffusion or arrested spreading effects predicted in Ref.⁴⁰.

For $\phi_0 > 1\%$, we observe a good agreement between the experimental curves for $\tau_{\max}(c_0)$ and the theoretical curves for $\tau^\dagger(c_0)$ in correspondence of values of α smaller than α_b (inset of Fig. 4(e)). More in detail, an increase in ϕ_0 of a factor 8 requires to reduce α by a factor 3-4 to attain a meaningful agreement with the experimental results. We attribute the observed behavior of the diffusiophoretic mobility coefficient to the neglect of inter-colloids interactions in Eqs. (1), an approximation only reasonable in diluted conditions where $\phi_0 \rightarrow 0$. At larger values of ϕ_0 , instead, when combined with the mapping procedure described above, this simplifying assumption leads to effective values of α that embed the contribution of the inter-colloids interactions. It seems that the latters, which are always present in experiments, are able to reduce the diffusiophoretic coupling $\alpha\phi\nabla c$. This reduction, however, does not affect the decrease of τ^\dagger when ϕ_0 is increased for fixed values of c_0 (Fig. 4(e)).

In summary, we demonstrate the existence of a novel convective instability occurring under isothermal conditions in a suspension of colloidal particles dispersed uniformly within a fluid mixture where the concentration of a molecular solute decreases with height. This result is surprising because the suspension is originally in a condition of stable mechanical equilibrium determined by having a heavier solute lying below a lighter solvent, and convective flows are consequently inhibited. The key point to understand this striking outcome

is the dominance, for single colloidal particles, of surface tension effects over gravitational and Brownian forces. To reduce the solute-colloid interfacial energy⁴¹, indeed, particles experience an upward diffusiophoretic motion which leads them to deplete from the bottom of the sample and to accumulate toward the top. Consequently, a mechanically unstable layer develops within the sample where the density of the suspension increases with height and a convective instability arises to minimize this localized rise in gravitational potential energy. Our results have significant implications for the control of pattern formation and for the handling of nanoparticles in inhomogeneous environments, and thus widespread applications in industrial, geological and biological systems. Understanding how the reported scenario varies under reduced gravity and hyper gravity conditions represents a future ambitious task of strategic relevance for space exploration^{42,43}.

Acknowledgement

Work partially supported by the European Space Agency (ESA) in the framework of the “Giant fluctuations”, NESTEX and “Sedimenting Colloids” projects, and by the Italian Space Agency (ASI) through the projects “Gravitationally Tapping Colloids in Space (GTACS) - Sedimenting Colloids” (Number 2023-19-U.0) and “Non-Equilibrium Phenomena in Soft Matter and Complex Fluids (NESTEX)” (Number 2023-20-U.0). A.Z. gratefully acknowledges funding from the European Union through Horizon Europe ERC Grant number: 101043968 “Multimech”, from US Army Research Office through contract nr. W911NF-22-2-0256, and from the Niedersächsische Akademie der Wissenschaften zu Göttingen in the frame of the Gauss Professorship program.

Supplementary Information

Convective patterns

Pattern formation has been investigated systematically for combinations of the colloid volume fraction ϕ_0 in the range $\{1\% - 8\%\}$ and of the concentration of glycerol c_0 in the range $\{7\% - 56\%\}$. In all the investigated cases convective patterns develop after a latency time. Figure 5 shows the patterns when they have reached maximum contrast. The time evolution of the contrast of the convective patterns shows the emergence of a separation of the colloid, followed by a mixing phase determined by the onset of transient convective motions (Fig. 6).

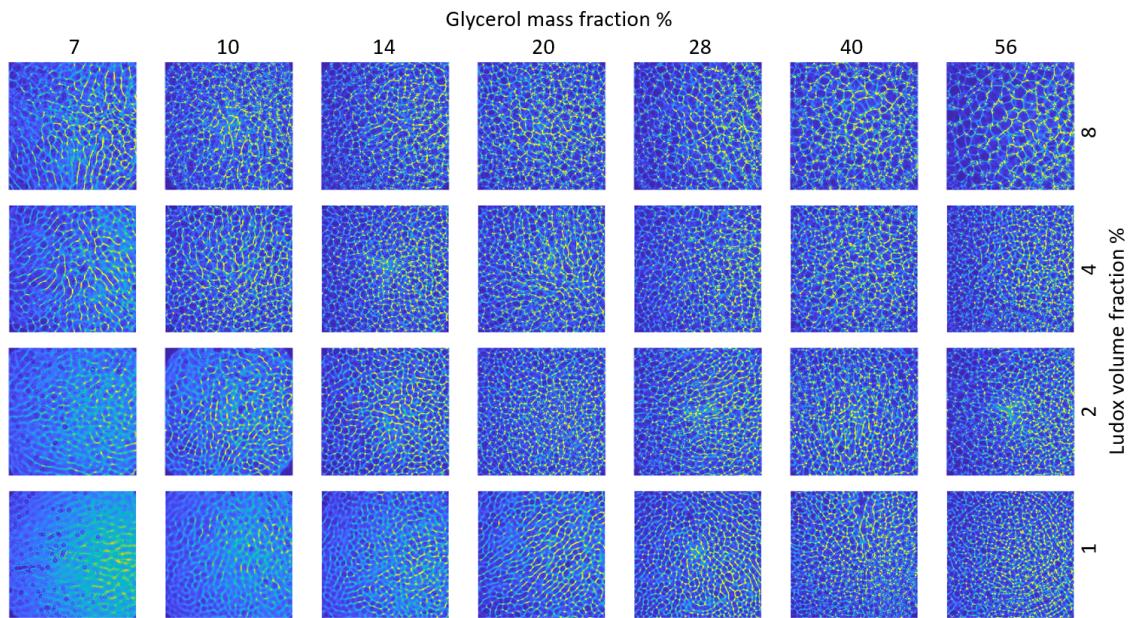


Figure 5: Shadowgraph images corresponding to the t_{\max} of Fig. 6. Each image shows the planform of the instability, at its maximum strength of intensity, to consist of a disordered cellular pattern. The panel of each image corresponds to 7.0 mm in real space.

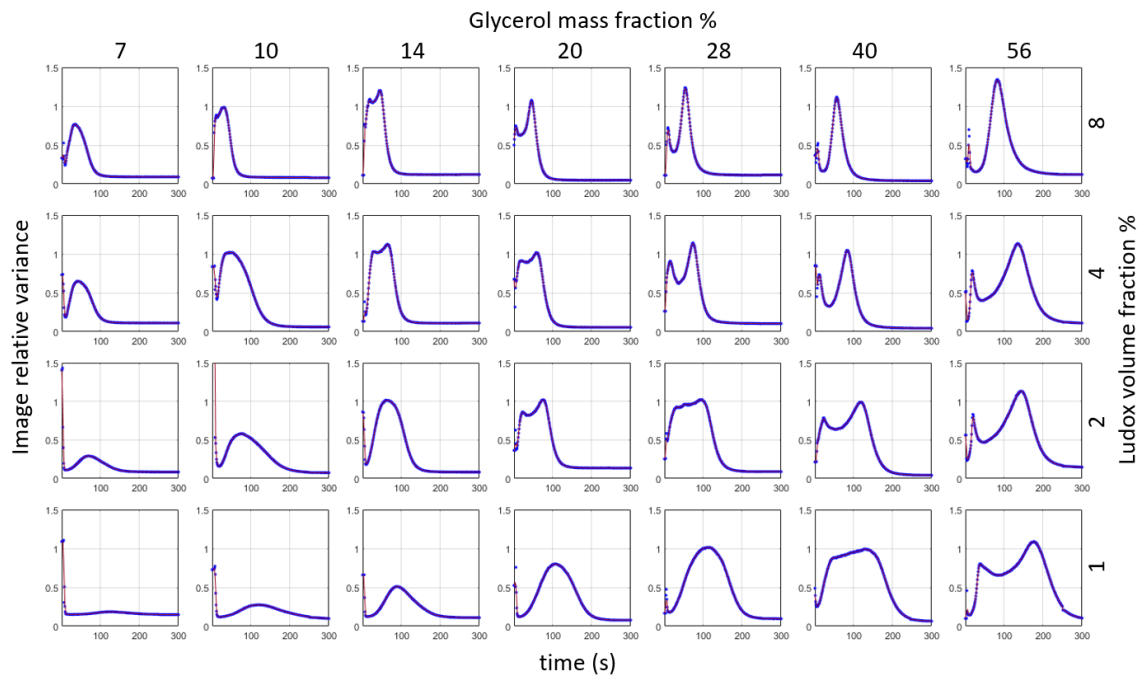


Figure 6: Temporal evolution of the relative variance for several values of the Ludox volume fraction and the glycerol mass fraction at time $t = 0$ (see main Letter). Each image shows the relative variance to increase until a maximum is reached at a time t_{\max} .

Theoretical model for the evolution of the base state

Diffusion coefficients

To solve Eqs. (1) of the main Letter, the ratio D_1/D_2 between the diffusion coefficients of glycerol in water, D_1 , and of colloidal spheres in a water-glycerol mixture, D_2 , has to be specified. In general, independently on the amount of dispersed colloids, these two coefficients are expected to vary as a function of the mass fraction of glycerol c_0 present in the bottom layer at $t = 0$ (see Fig. 1 of the main Letter). We recall that experimental values of this latter quantity are used as initial conditions in our theoretical model. For any given value of c_0 , the glycerol mass fraction c varies along the (vertical) z direction (see Fig. 4(a) of the main Letter) and, consequently, multiple values of c exist which could be exploited to fix the values of D_1 and D_2 corresponding to that c_0 . To deal with this issue, we adopt the following strategy: for any given value of c_0 , we compute D_1 and D_2 at $\bar{c} = c_0/2$. In other words, we fix $D_1 \equiv D_1(\bar{c})$ and $D_2 \equiv D_2(\bar{c})$.

We extrapolate values of D_1 from Ref.³⁵. Instead, we compute D_2 by means of the Stokes-Einstein formula

$$D_2 = \frac{k_B T}{6\pi\eta a}. \quad (2)$$

Here k_B is the Boltzmann constant, T is the temperature, a is the radius of the diffusing colloids and η is the viscosity of the water-glycerol mixture. From Eq. (2), it is clear that the dependence of D_2 on c_0 is embedded in the dependence of η on c_0 . Again, for any c_0 , the corresponding value of the viscosity is fixed to $\eta \equiv \eta(\bar{c})$ where $\bar{c} = c_0/2$. We extract η from data concerning a water-glycerol mixture at $T = 20^\circ$ reported in Ref.⁴⁴ To compute D_2 we recall that $a = 11$ nm in our experimental system.

For all the values of c_0 considered in our experiments, while D_1 and D_2 individually vary as a function of c_0 , their ratio remains constant $D_1/D_2 \approx 100$. This is the value which is used to solve Eqs. (1) of the main Letter.

Density profile

The mass density ρ of our system is a function of the position \mathbf{r} and of the time t . i. e. $\rho \equiv \rho(\mathbf{r}, t)$. At a fixed time t , the total mass of fluid present in an elementary volume element V centered at \mathbf{r} is given by $M = M_L + M_B$, where M_L and $M_B = M_{\text{water}} + M_{\text{glycerol}}$ are the masses of the Ludox particles and of the binary water-glycerol mixture contained in V , respectively. It follows that

$$\rho \equiv \frac{M}{V} = \frac{M_L}{V} + \frac{M_B}{V}. \quad (3)$$

Calling N_L the number of Ludox particles contained in V , and m_L their mass, it follows that $M_L = N_L m_L$. Moreover, calling v_L the volume of each colloid, the volume V_L occupied by the Ludox particles within V can be written as $V_L = N_L v_L$. It follows that the term M_L/V in Eq. (3) can be written as

$$\frac{M_L}{V} = \phi \rho_L, \quad (4)$$

where $\phi \equiv V_L/V$ is the colloid volume fraction and $\rho_L \equiv m_L/v_L$ is the density of a single colloidal particle.

To determine the term M_B/V in Eq. (3), we notice that the part of V available for the water molecules and the glycerol particles is $V_B = V - V_L$. It follows that the density of the water-glycerol mixture is $\rho_B = M/(V - V_L)$, and that

$$\frac{M_B}{V} = \rho_B \frac{V - V_L}{V} = \rho_B (1 - \phi). \quad (5)$$

Inserting Eqs. (4) and (5) into Eq. (3) we obtain

$$\rho = (\rho_L - \rho_B)\phi + \rho_B. \quad (6)$$

Since ρ_B is a function of c , the dependence of ρ on c in Eq. (6) is contained in ρ_B . Experi-

mental data from Ref.⁴⁴ show that ρ_B exhibits a nearly linear dependence on c :

$$\rho_B = \rho_0 + \beta c, \quad (7)$$

where ρ_0 is the density of the solvent in the absence of glycerol molecules, and $\beta \equiv d\rho_B/dc$ is the solutal expansion coefficient of a water-glycerol mixture of density ρ_B .

Inserting Eq. (7) into Eq. (6), we get

$$\rho(c, \phi) = \rho_0 + (\rho_L - \rho_0)\phi + \beta(1 - \phi)c. \quad (8)$$

To take into account small deviations from linearity of the experimental data of Ref.⁴⁴, in Eq. S7 we assume that β depends on c_0 . We characterize this dependence through a fit of the data from Ref.⁴⁴ in the concentration range $[0, c_0]$. Slightly different values of β are obtained by varying c_0 , which are listed in Table 1. To check the consistency of this method, during the fitting procedure we also leave ρ_0 as a free parameter and, as expected, we obtain a nearly constant value of ρ_0 , corresponding to the density of pure water (Table 1). The values of ρ_0 and β are assumed to be independent on ϕ_0 .

Table 1: Values of ρ_0 and β in Eq. (8) as a function of c_0 . The values are obtained through a fit to data from Ref.⁴⁴ in the concentration range $[0, c_0]$.

c_0 [%]	ρ_0 [g cm ⁻³]	β [g cm ⁻³]
7	0.9982	0.2305
10	0.9982	0.2332
14	0.9981	0.2340
20	0.9979	0.2376
28	0.9977	0.2418
40	0.9972	0.2487
56	0.9965	0.2554

References

- (1) Derjaguin, B.; Sidorenkov, G.; Zubashchenko, E.; Kiseleva, E. Kinetic Phenomena in the boundary layers of liquids 1. the capillary osmosis. *Kolloidnyj Zhurnal* **1947**, *9*, 335–347.
- (2) Derjaguin, B.; Sidorenkov, G.; Zubashchenko, E.; Kiseleva, E. Kinetic Phenomena in the boundary layers of liquids 1. the capillary osmosis. *Prog. Surf. Sci.* **1993**, *43*, 138–152.
- (3) Anderson, J. L. Colloid Transport by Interfacial Forces. *Annu. Rev. Fluid Mech.* **1989**, *21*, 61–99.
- (4) Anderson, J. L.; Prieve, D. C. Diffusiophoresis: Migration of Colloidal Particles in Gradients of Solute Concentration. *Sep. Purif. Methods* **1984**, *13*, 67–103.
- (5) Palacci, J.; Abécassis, B.; Cottin-Bizonne, C.; Ybert, C.; Bocquet, L. Colloidal Motility and Pattern Formation under Rectified Diffusiophoresis. *Phys. Rev. Lett.* **2010**, *104*, 138302.
- (6) Shin, S. Diffusiophoretic separation of colloids in microfluidic flows. *Phys. Fluids* **2020**, *32*, 101302.
- (7) Shklyaev, O. E.; Shum, H.; Balazs, A. C. Using Chemical Pumps and Motors To Design Flows for Directed Particle Assembly. *Acc. Chem. Res.* **2018**, *51*, 2672–2680.
- (8) Golestanian, R.; Liverpool, T. B.; Ajdari, A. Propulsion of a Molecular Machine by Asymmetric Distribution of Reaction Products. *Phys. Rev. Lett.* **2005**, *94*, 220801.
- (9) Golestanian, R.; Liverpool, T. B.; Ajdari, A. Designing phoretic micro- and nano-swimmers. *New J. Phys.* **2007**, *9*, 126–126.
- (10) Moran, J. L.; Posner, J. D. Phoretic Self-Propulsion. *Annu. Rev. Fluid Mech.* **2017**, *49*, 511–540.

- (11) Shin, S.; Ault, J. T.; Warren, P. B.; Stone, H. A. Accumulation of Colloidal Particles in Flow Junctions Induced by Fluid Flow and Diffusiophoresis. *Phys. Rev. X* **2017**, *7*, 041038.
- (12) Kar, A.; Chiang, T.-Y.; Ortiz Rivera, I.; Sen, A.; Velegol, D. Enhanced Transport into and out of Dead-End Pores. *ACS Nano* **2015**, *9*, 746–753.
- (13) Shin, S.; Um, E.; Sabass, B.; Ault, J. T.; Rahimi, M.; Warren, P. B.; Stone, H. A. Size-dependent control of colloid transport via solute gradients in dead-end channels. *PNAS* **2016**, *113*, 257–261.
- (14) Akdeniz, B.; Wood, J. A.; Lammertink, R. G. H. Diffusiophoresis and Diffusio-osmosis into a Dead-End Channel: Role of the Concentration-Dependence of Zeta Potential. *Langmuir* **2023**, *39*, 2322–2332.
- (15) Singh, N.; Vladisavljević, G. T.; Nadal, F.; Cottin-Bizonne, C.; Pirat, C.; Bolognesi, G. Reversible Trapping of Colloids in Microgrooved Channels via Diffusiophoresis under Steady-State Solute Gradients. *Phys. Rev. Lett.* **2020**, *125*, 248002.
- (16) Shi, N.; Nery-Azevedo, R.; Abdel-Fattah, A. I.; Squires, T. M. Diffusiophoretic Focusing of Suspended Colloids. *Phys. Rev. Lett.* **2016**, *117*, 258001.
- (17) Chen, Y.; Chong, K. L.; Liu, L.; Verzicco, R.; Lohse, D. Instabilities driven by diffusiophoretic flow on catalytic surfaces. *J. Fluid Mech.* **2021**, *919*, A10.
- (18) Alessio, B. M.; Gupta, A. Diffusiophoresis-enhanced Turing patterns. *Sci. Adv.* **2023**, *9*, eadj2457.
- (19) Ramm, B.; Goychuk, A.; Khmelinskaia, A.; Blumhardt, P.; Eto, H.; Ganzinger, K. A.; Frey, E.; Schwille, P. A diffusiophoretic mechanism for ATP-driven transport without motor proteins. *Nat. Phys.* **2021**, *17*, 850–858.
- (20) Oster, G.; Yamamoto, M. Density Gradient Techniques. *Chem. Rev.* **1963**, *63*, 257–268.

- (21) Castellini, S.; Carpineti, M.; Giraudet, C.; Croccolo, F.; Vailati, A. Dynamics of non-equilibrium concentration fluctuations during free-diffusion in highly stratified solutions of glycerol and water. *The Journal of Chemical Physics* **2023**, *158*.
- (22) Landau, L.; Lifshitz, E. *Fluid Mechanics: Volume 6*; Elsevier Science, 2013.
- (23) Righetti, P. G.; Bossi, A.; Giglio, M.; Vailati, A.; Lyubimova, T.; Briskman, V. A. Is gravity on our way? The case of polyacrylamide gel polymerization. *Electrophoresis* **1994**, *15*, 1005–1013.
- (24) Normand, C.; Pomeau, Y.; Velarde, M. G. Convective instability: A physicist’s approach. *Rev. Mod. Phys.* **1977**, *49*, 581–624.
- (25) Veronis, G. Effect of a stabilizing gradient of solute on thermal convection. *J. Fluid Mech.* **1968**, *34*, 315–336.
- (26) Trevelyan, P. M. J.; Almarcha, C.; De Wit, A. Buoyancy-driven instabilities of miscible two-layer stratifications in porous media and Hele-Shaw cells. *J. Fluid Mech.* **2011**, *670*, 38–65.
- (27) Giavazzi, F.; Savorana, G.; Vailati, A.; Cerbino, R. Structure and dynamics of concentration fluctuations in a non-equilibrium dense colloidal suspension. *Soft Matter* **2016**, *12*, 6588–6600.
- (28) De Gennes, P.-G.; Brochard-Wyart, F.; Quéré, D. *Capillarity and wetting phenomena: drops, bubbles, pearls, waves*; Springer: New York, NY, 2004.
- (29) Settles, G. S. *Schlieren and Shadowgraph Techniques*; Springer, 2001.
- (30) See Supplemental Information at URL..., presenting additional figures and technical details on the model.

- (31) Cerbino, R.; Vailati, A.; Giglio, M. Soret driven convection in a colloidal solution heated from above at very large solutal Rayleigh number. *Phys. Rev. E* **2002**, *66*, 055301(R).
- (32) Anderson, J. L.; Lowell, M. E.; Prieve, D. C. Motion of a particle generated by chemical gradients Part 1. Non-electrolytes. *J. Fluid Mech.* **1982**, *117*, 107–121.
- (33) Raj, R. R.; Shields, C. W.; Gupta, A. Two-dimensional diffusiophoretic colloidal banding: optimizing the spatial and temporal design of solute sinks and sources. *Soft Matter* **2023**, *19*, 892–904.
- (34) At any time τ , the top equation of Eqs. (1) is solved analytically (via separation of variables⁴⁵). After insertion of the obtained $c(z, \tau)$, the bottom equation of Eqs. (1) is solved numerically (via finite difference method^{45,46}) to compute $\phi(z, \tau)$.
- (35) Nishijima, Y.; Oster, G. Diffusion in Glycerol-Water Mixture. *Bull. Chem. Soc. Jpn.* **1960**, *33*, 1649–1651.
- (36) We use data from Ref.³⁵ to fix D_1 and the Stokes-Einstein formula to compute $D_2 = k_B T / (6\pi\eta a)$, where k_B is the Boltzmann constant, $a = 11$ nm the radius of the colloidal particles, and for the shear viscosity η of the water-glycerol mixture we use data collected at $T = 20^\circ\text{C}$ ⁴⁴. D_1 and D_2 vary individually as a function of c_0 , however their ratio remains constant to $D_1/D_2 \approx 100$ for any given glycerol mass fraction. The coefficients ρ_0 and β in the expression to compute the density profile of the suspension are obtained through a fit of data from Ref.⁴⁴. Slightly different values are obtained by varying c_0 , which are listed in Table S1 of the SI³⁰. The values of D_1 , D_2 , ρ_0 and β never depend on ϕ_0 .
- (37) Squires, T. M.; Quake, S. R. Microfluidics: Fluid physics at the nanoliter scale. *Rev. Mod. Phys.* **2005**, *77*, 977–1026.
- (38) Messlinger, S.; Schöpf, W.; Rehberg, I. Transient diffusive boundary layers at high

- Rayleigh numbers in simple and double diffusive fluids: Latency time scaling for the convection onset. *Int. J. Heat Mass Transf.* **2013**, *62*, 336–349.
- (39) Gupta, A.; Shim, S.; Stone, H. A. Diffusiophoresis: from dilute to concentrated electrolytes. *Soft Matter* **2020**, *16*, 6975–6984.
- (40) Chu, H. C. W.; Garoff, S.; Tilton, R. D.; Khair, A. S. Advective-diffusive spreading of diffusiophoretic colloids under transient solute gradients. *Soft Matter* **2020**, *16*, 238–246.
- (41) Ruckenstein, E. Can phoretic motions be treated as interfacial tension gradient driven phenomena? *J. Colloid Interface Sci.* **1981**, *83*, 77–81.
- (42) Vailati, A. et al. Diffusion in liquid mixtures. *NPJ Microgravity* **2023**, *9*.
- (43) Vailati, A.; Šeta, B.; Bou-Ali, M.; Shevtsova, V. Perspective of research on diffusion: From microgravity to space exploration. *Int. J. Heat Mass Transf.* **2024**, *229*, 125705.
- (44) Lide, D. *CRC Handbook of Chemistry and Physics*, *85th Edition*; CRC Handbook of Chemistry and Physics, 85th Ed v. 85; Taylor & Francis, 2004.
- (45) Crank, J. *The Mathematics of Diffusion*; Oxford University: Oxford, 1975.
- (46) Smith, G. *Numerical Solution of Partial Differential Equations: Finite Difference Methods*; Oxford applied mathematics and computing science series; Clarendon Press, 1985.

TOC Graphic

